Evolution of extreme events in a semiconductor laser subject to chaotic optical injection

Yu Huang,* Pei Zhou,* Yao Zeng, Renheng Zhang, and Nianqiang Li†
School of Optoelectronic Science and Engineering and Collaborative Innovation Center of Suzhou Nano Science and Technology, Soochow University, Suzhou 215006, China
and Key Lab of Advanced Optical Manufacturing Technologies of Jiangsu Province and Key Lab of Modern Optical Technologies of the Education Ministry of China, Soochow University, Suzhou 215006, China

(Received 15 January 2022; revised 23 March 2022; accepted 15 April 2022; published 26 April 2022)

Extreme events (EEs) are rare and unexpected events that emerge in many natural systems and are the object of intensive studies. Here, we experimentally investigate the evolution of deterministic optical EEs in a slave laser (SL) subject to chaotic optical injection from a master laser (ML) with optical feedback. Although the ML operates in the long-cavity regime, we observe occasional pulses that are high enough to be considered EEs, and the appearance probability of EEs can be significantly enhanced in the SL for certain injection parameters outside the injection-locking regions of the master-slave configuration. Additionally, the evolution of EEs can be readily identified from the two-dimensional maps. The numerical results show good qualitative agreement with the experiment. These results reveal the importance of injection parameters for the appearance of EEs in chaotic lasers and can be easily extended to other coupled systems.

DOI: 10.1103/PhysRevA.105.043521

I. INTRODUCTION

In nature, many physical systems display the behavior of extreme events (EEs) that can significantly impact their surroundings. A typical example of such behavior is the unexpected appearance of destructive oceanic rogue waves (RWs) in a calm sea [1,2]. The intrinsic scarcity and the evident technical difficulties in the implementation of experiments have been the major challenges to understanding the generation of RWs. In 2007, a useful test platform was proposed that leveraged an analogy between ocean RWs and light fields with ultrahigh intensity but extremely low probability in the process of supercontinuum generation in optical fibers, which were termed optical RWs [3]. This pioneering result has widely flourished in studies of EEs and essentially opened up a novel field of "optical RWs physics" [4–9].

Recently, optical RWs have been investigated in deterministic optical systems due to their significant effects in the real world [10–20]. For example, in the telecommunication data field, the appearance of extreme pulses will restrict the speed of optical communication links. On the contrary, high-amplitude pulses that appear on demand can be used as ideal light sources for special applications, such as imaging and sensing. Therefore, much effort has been devoted to understanding the formation mechanism of EEs and, if possible, controlling them, achieving desirable environments and systems. For example, Masoller *et al.* revealed the formation of extreme pulses originated from an external crisislike process in the continuous-wave optical injection semiconductor laser (cw-OISL) system and demonstrated that optical RWs can be predicted with a long anticipation time [21,22]. Perrone *et al.* predicted that the extreme pulse can be suppressed by using direct current modulation in the same cw-OISL system [23]. Moreover, these results have shown that noise can significantly affect the generation probability of EEs. Interestingly, Jin *et al.* numerically demonstrated that the high-amplitude extreme pulse can be motivated with more than 50% probability on demand by a step-up perturbation of the laser current [24]. These studies of EEs are beneficial to improving the performance of lasers for different applications. It should be noted that EEs are found in only the slave laser (SL) in the cw-OISL system since the master laser (ML) outputs cw light. On the other hand, the external perturbation can drive the ML to operate in chaotic regimes. EEs were found in a semiconductor laser with a short external cavity, accompanied by deterministic intermittency [17], and a slightly long external cavity due to low-frequency fluctuations [12], as well as in a semiconductor laser with phase-conjugate optical feedback [11]. The long-cavity regime means that the external-cavity round-trip time is much longer than the laser relaxation oscillation period. It is well known that the external cavity length plays an important role in determining the route to chaos and significantly complicates the dynamic behavior of the laser. In the literature, in spite of the fact that the nonlinear dynamics of semiconductor lasers with optical feedback in the long-cavity regime and their applications have received considerable attention [25–27], the fact that they can generate giant pulses that are high enough to be considered as EEs has not yet been reported systematically. In addition, it is of interest to know whether the occurrence probability of EEs generated by an ML can be enhanced or decreased in the SL by tailoring chaotic optical injection.

In this paper, we study the evolution of EEs in a semiconductor laser subject to chaotic optical injection. Here, we

*These authors contributed equally to this work.
†Corresponding author: wan_103301@163.com

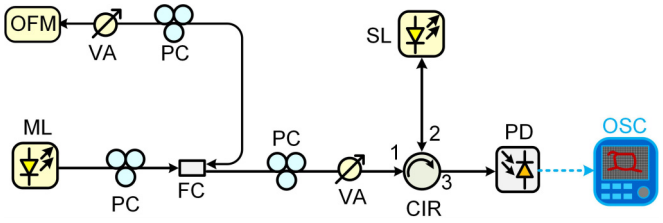

FIG. 1. Experimental setup. ML: master laser; SL: slave laser; FC: fiber coupler; PC: polarization controller; OFM: optical-fiber mirror; VA: variable attenuator; CIR: optical circulator; PD: photodetector; OSC: oscilloscope.

select an ML with optical feedback in the long-cavity regime as the chaotic source and study the generation of EEs. In the previous reports, the origin, predictability, and suppression of optical EEs were discussed in cw-OISLs [21,22], whereas we focus on the evolution of EEs in an SL under an external force, i.e., the chaotic optical injection from the ML. Such a system can achieve a broad and accessible chaotic regime to investigate the evolution of EEs and provide more insights into the control of EEs. We investigate the evolution of EEs in the injection-parameter space and observe that the generation probability of EEs can be significantly enhanced in selected injection-parameter regions. In addition, we also find that the injection-locking effect plays an important role in the evolution of EEs. Our experimental observations are also supported by numerical investigations. Such a phenomenon is of interest for experimental and theoretical investigations of EEs in other natural systems in which a similar response to external forcing can be found.

This paper is organized as follows. In Sec. II, we show our experimental setup for observing the evolution of EEs in the master-slave-configuration semiconductor-laser system. The associated theoretical frameworks are described in Sec. III to gain further insight into the experimental observations. In Sec. IV, we carefully illustrate the experimental and theoretical results for the EEs. Finally, our conclusions are summarized in Sec. V.

II. EXPERIMENT SETUP

Figure 1 displays the experimental setup of EEs in a semiconductor laser subject to chaotic optical injection. In this implementation, two commercial distributed feedback (DFB) semiconductor lasers (Wuhan 69 Inc.) are deployed. Two lasers with a threshold current of approximately 12 mA are driven and controlled by a current source and a thermoelectric controller. One laser is selected as the ML with a bias current of 25 mA and a fixed temperature of 25 °C, which leads to a lasing wavelength of 1551.173 nm. The other laser acts as the SL with a bias current of 18 mA, while its temperature is adjusted in real time to form the frequency detuning $\Delta f = f_{\mathrm{ML}} - f_{\mathrm{SL}}$ between the ML and the SL, where f_{ML} and f_{SL} denote the center frequencies of the free-running ML and SL, respectively. The ML is connected to an optical feedback loop consisting of the fiber coupler (FC), polarization controller (PC), variable attenuator (VA), and optical-fiber mirror for chaos generation, where the resulting feedback delay time is approximately 112 ns and is apparently much larger than the laser relaxation oscillation period. Then, the chaotic signal is injected into the SL through the same FC, PC, and VA and optical circulator. The feedback power P_f and injection power P_i can be separately changed by VAs. Under the selected parameters, the SL generates the chaotic signal, which is transmitted into a photodetector (HP 11982A, bandwidth of 15 GHz) for photoelectric transformation. Finally, the data can be acquired from the oscilloscope (LeCroy WaveMaster820Zi-B, sampling rate of 80 GS/s, bandwidth of 20 GHz).

III. THEORETICAL MODEL

In this work, we also simulate the theoretical model to further understand our experimental results. Based on the Lang-Kobayashi model, the rate equations of the ML configuration can be written as [28]

$$\frac{dE_M(t)}{dt} = \frac{1+i\alpha}{2}\left[G_M - \frac{1}{\tau_p}\right]E_M(t) + k_f E_M(t-\tau_f)\exp(-i2\pi f_M \tau_f), \tag{1}$$

$$\frac{dN_M(t)}{dt} = \frac{J_M}{q} - \frac{N_M}{\tau_e} - G_M(t)|E_M|^2 \tag{2}$$

$$G_M(t) = \frac{g[N_M(t) - N_0]}{1+\varepsilon|E_M(t)|^2}, \tag{3}$$

and the rate equations of the SL can be written as

$$\frac{dE_S(t)}{dt} = \frac{1+i\alpha}{2}\left[G_S - \frac{1}{\tau_p}\right]E_S(t) + k_{\mathrm{inj}}E_M(t-\tau_c)\exp\left[-i(2\pi f_M \tau_c - 2\pi\Delta f t)\right], \tag{4}$$

$$\frac{dN_S(t)}{dt} = \frac{J_S}{q} - \frac{N_{M,S}}{\tau_e} - G_S(t)|E_S|^2 \tag{5}$$

$$G_S(t) = \frac{g[N_S(t) - N_0]}{1+\varepsilon|E_S(t)|^2}, \tag{6}$$

where the subscripts M and S denote the ML and SL, respectively. $E(t)$ and $N(t)$ are the slowly varying complex electric field and carrier number. The parameters of the model are defined as follows: G is the optical gain, g is the gain coefficient, ε is the saturation coefficient, α is the linewidth enhancement factor, N_0 is the carrier density at transparency, τ_p is the photon lifetime, τ_e is the carrier lifetime, and J is the bias current (J_{th} is the threshold current). The feedback parameters contain the feedback strength k_f, feedback delay time τ_f, and the center frequency of the ML f_M. The injection parameters include the injection strength k_{inj}, injection delay time τ_c, and the frequency detuning Δf, which are consistent with the definition in the experiment. Here, we use a fourth-order Runge-Kutta algorithm to solve Eqs. (1)–(6) with a time step of 1 ps. The parameter values of lasers are set as $g = 1.5 \times 10^4$, $\alpha = 5$, $N_0 = 1.5 \times 10^8$, $\varepsilon = 1.5 \times 10^{-7}$, $\tau_p = 2$ ps, $\tau_e = 2$ ns, $\tau_c = 2$ ns, $k_f = 16\ \mathrm{ns}^{-1}$, $\tau_f = 3$ ns, $J_M = 2.08J_{\mathrm{th}}$, $J_S = 1.5J_{\mathrm{th}}$, $J_{\mathrm{th}} = 14.7$ mA, and $f_M = 193.55$ THz [28]. Moreover, the quantity of electric charge $q = 1.602 \times 10^{-19}$ C. The relaxation oscillation frequency of the free-running laser is defined as $f_{\mathrm{RO}} = 1/(2\pi)[(J/J_{\mathrm{th}} - 1)/(\tau_N\tau_p)(1 + gN_0\tau_p)]^{1/2}$ [29]. For a bias current $J = 2.08J_{\mathrm{th}}$, the ML has a relaxation oscilla-

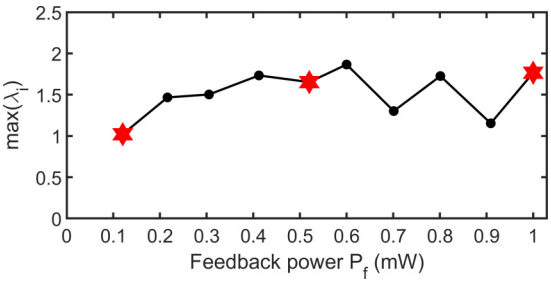

FIG. 2. Largest Lyapunov exponent max(λ_i) as a function of feedback power P_f. Red stars are selected to calculate the occurrence probability of EEs in Fig. 3.

tion frequency of 5.98 GHz, and the corresponding relaxation oscillation period is 0.167 ns, which is much smaller than the delay time and thus confirms the long-cavity operation. Our simulations are performed with a time duration of 11 μs, but only the time series in the last 10 μs are used to calculate the probability of EEs. Likewise, the experimental data are recorded for 10 μs with a sampling rate of 80 GS/s to compute the results.

To confirm the EEs, we use a common criterion abnormality index I_A, which was widely used in previous studies of optical RWs [30,31]. Each event E_n has an $I_{A,n}$, which is defined as

$$I_{A,n} = Hf_n/H_{1/3}.$$

In this expression, Hf_n stands for the peak height of all events of time series, and $H_{1/3}$ denotes the average value of the third of the highest values of Hf_n. When $I_{A,n} \geqslant 2$ the event is identified as an EE. Moreover, the probability density functions of the peak intensity are plotted to observe the evolution of EEs [21,32].

IV. RESULTS AND DISCUSSION

In this work, we want to reveal the effects of the injection parameters, i.e., frequency detuning and injection strength, on the evaluation of EEs. First of all, we experimentally investigate the occurrence of EEs in the ML in the long-cavity regime, which is used as a chaotic injection signal source. To confirm the dynamic state of the ML, we calculate the largest Lyapunov exponent (LLF) [33] using the experimental data, and the results are shown in Fig. 2. It can be seen that the LLFs are strictly positive when the feedback power P_f is larger than 0.12 mW. This demonstrates that the ML indeed works in the chaotic regimes for the feedback powers chosen. We further show the representative examples of EEs generated from the ML with three selected optical feedback powers P_f, where $P_i = 0$. In Fig. 3(a1), weak feedback is applied in the ML with $P_f = 0.12$ mW. From the zoom of the intensity time trace, we see that the output of the ML presents an irregular oscillation. The occurrence probability of EEs is counted as 0% within the intensity time series of 10 μs. Further, the probability of the peak intensity is plotted in Fig. 3(b1). From this plot, we can see that the probability of events with the peak beyond the threshold of EEs is zero. In Fig. 3(a2), P_f is enhanced to 0.52 mW, the EEs can be found in the zoom of the intensity time trace, and the occurrence probability of EEs is increased

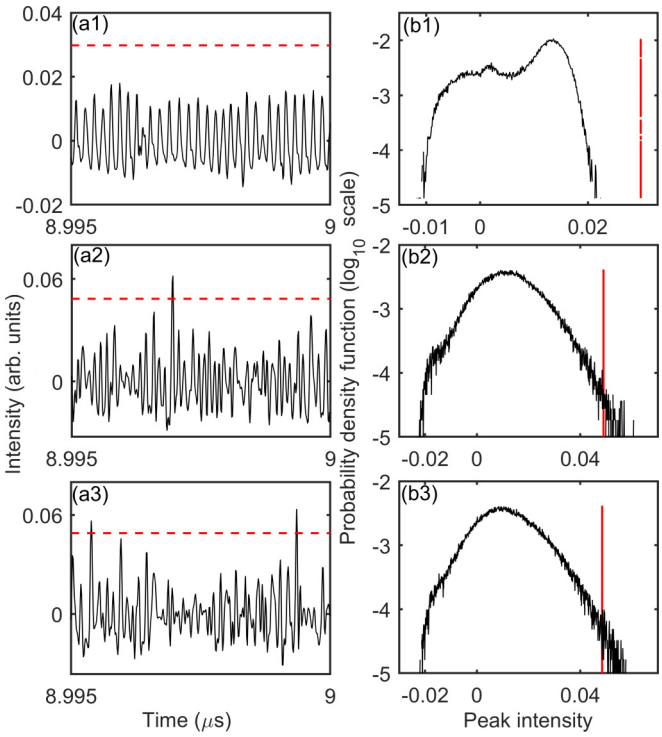

FIG. 3. Chaotic time series and statistical distributions of ML with optical feedback observed in the experiment, where (a1) and (b1) $P_f = 0.12$ mW, (a2) and (b2) $P_f = 0.52$ mW, and (a3) and (b3) $P_f = 1$ mW. Red dashed lines and vertical solid lines represent an abnormality index of 2.

to 0.170% in the window of 10 μs. The corresponding statistical distribution is asymmetric (above the I_A threshold) on the right side, as shown in Fig. 3(b2). In Fig. 3(a3), we further improve P_f to 1 mW, and the occurrence of EEs is more frequent. Quantitatively, the occurrence probability of EEs is enlarged to 0.257%. Intuitively, the probability of events with the peak beyond the threshold of EEs also increases [see Fig. 3(b3)]. These results indicate that the occurrence probability of EEs can be enhanced by increasing the feedback power. A similar evolution has been found in DFB lasers with phase-conjugate feedback and vertical-cavity surface-emitting lasers (VCSELs) with conventional optical feedback [13,34].

With the above observations, we confirm that EEs can occur in the ML with optical feedback in the long-cavity regime, but such a phenomenon is less observed than the short-cavity case [17]. Now, we turn to discussing the appearance of EEs in the SL subject to chaotic optical injection. Here, we choose a moderate value of $P_f = 0.52$ mW and show typical examples of EEs for normalized injection strength $\gamma = 0.1$ (where γ is defined as the proportional amplitude of the light injected to the SL) and three different settings of the frequency detuning Δf. For the three detuning cases ($\Delta f = 30$, 0, and -20 GHz), the associated LLFs are calculated as 1.23, 1.65, and 2.56, respectively. Figure 3(a1) depicts the zoom of the time series when the frequency detuning Δf is 30 GHz. By comparing Figs. 3(a2) and 4(a1), we can see that a faster dynamic pulsation is found in the output of the SL and results in more events over the threshold. The occurrence probability of EEs is calculated to be 1.637% in the window of 10 μs. The probability

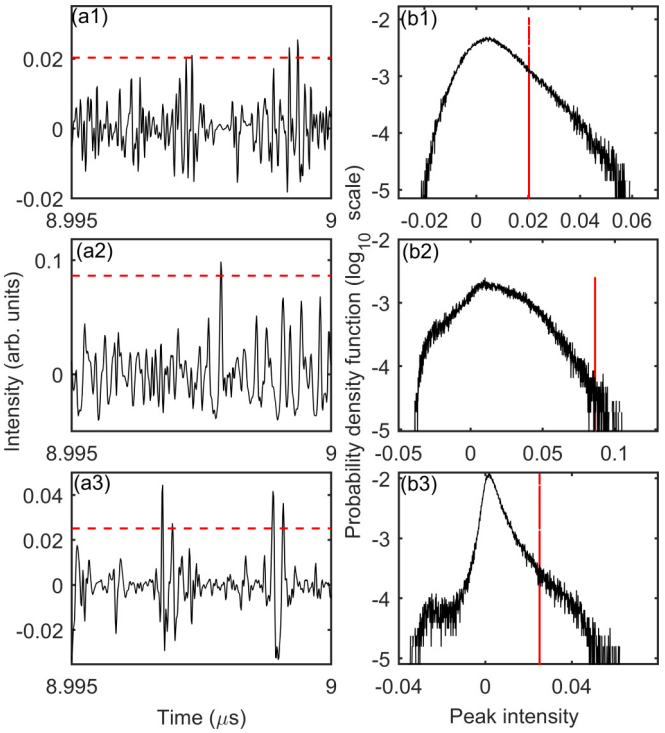

FIG. 4. Chaotic time series and statistical distributions of SL with chaotic optical injection observed in the experiment, where $P_f = 0.52$ mW, $\gamma = 0.1$, and (a1) and (b1) $\Delta f = 30$ GHz, (a2) and (b2) $\Delta f = 0$ GHz, and (a3) and (b3) $\Delta f = -20$ GHz. Red dashed lines and vertical solid lines represent an abnormality index of 2.

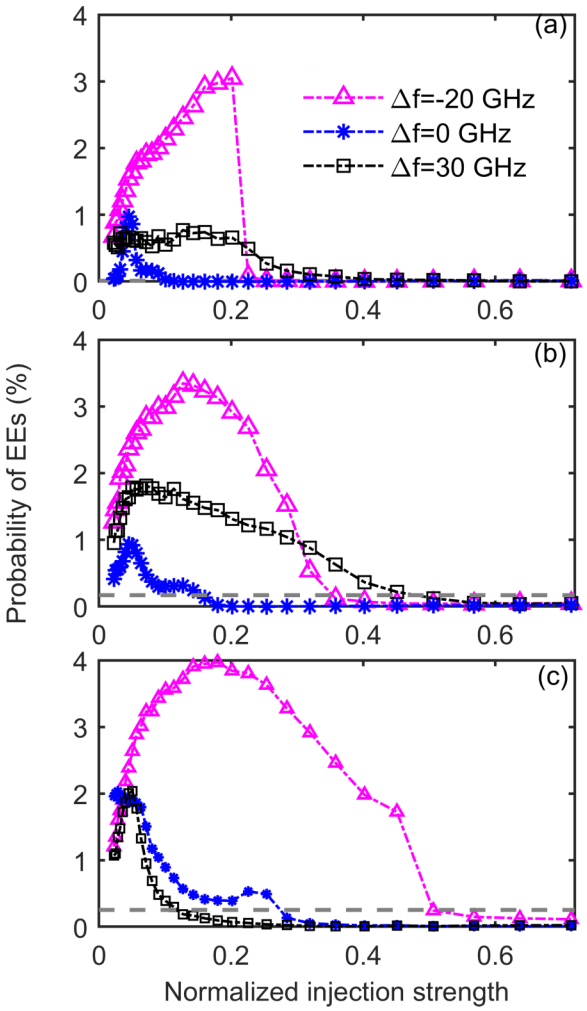

FIG. 5. The occurrence probability of EEs versus the normalized injection strength γ observed in the experiment, where (a) $P_f = 0.12$ mW, (b) $P_f = 0.52$ mW, and (c) $P_f = 1$ mW. Gray lines represent the probability of EEs generated from the ML.

of events with the peak beyond the threshold of EEs increases significantly compared with the case of the ML, as shown in Fig. 4(b1). When the frequency detuning is reduced to $\Delta f = 0$ GHz, the output intensity of the SL [see Fig. 4(a2)] shows a similar irregular oscillation compared with Fig. 3(a2). The occurrence probability of EEs is calculated as 0.301%, and a small probability of events with the peak beyond the threshold of EEs is observed in Fig. 4(b2). Compared with the case of the ML, the number of EEs increases slightly. When the frequency detuning is adjusted to $\Delta f = -20$ GHz, the feature of the long tail is obviously displayed in Fig. 4(b3), where the corresponding occurrence probability of EEs is 2.987%. From these results, we find that the variation of injection parameters can significantly affect the generation of EEs.

Next, we want to study how the behavior of EEs evolves for the SL when the normalized injection strength is used as the control parameter. Consequently, we show the results for the occurrence probability of EEs as a function of the normalized injection strength γ for $\Delta f \in [-20, 30]$ GHz and $P_f \in [0.12, 1]$ mW in Fig. 5. From Fig. 5, several interesting characters can be identified. First, for three cases of Δf, the generation probability of EEs is increased first and then decreased with the increase of γ and finally trends to stationary values. These stationary trends are attributed to the fact that the injection-locking mechanism is triggered, which is widely witnessed in the master-slave configuration [35,36]. Moreover, we can find that the stationary value is below the gray line under the cases of $\Delta f = 0$ GHz and $\Delta f = -20$ GHz, which means that the occurrence probability of EEs is decreased. Second, before the injection locking is triggered, windows for the enhanced EEs (over the gray line) can be observed for three cases of Δf. Also, for the selected value of γ, the generation probability of EEs in the case of $\Delta f = -20$ GHz is dramatically larger than that in the other cases. Third, for the cases of $\Delta f = 0$ and $\Delta f = -20$ GHz, the windows for the enhanced EEs are expanded as the feedback power is improved. However, for the case of $\Delta f = 30$ GHz, the window for the enhanced EEs expands first and then shrinks in size with the increase of the feedback power. This phenomenon will be discussed below.

To gain a global view of the EEs and the effects of injection parameters, we plot two-dimensional maps in the plane of Δf and γ with the variation of feedback power, as shown in Fig. 6. Here, the colors correspond to the occurrence probability of EEs generated from the SL. From Fig. 6(a), where $P_f = 0.12$ mW, it can be seen that two bright regions can be found in cases of both positive and negative detuning, which implies that the generation probability of EEs is significantly increased. In addition, asymmetry behavior with respect to zero detuning which originates from the nonzero linewidth

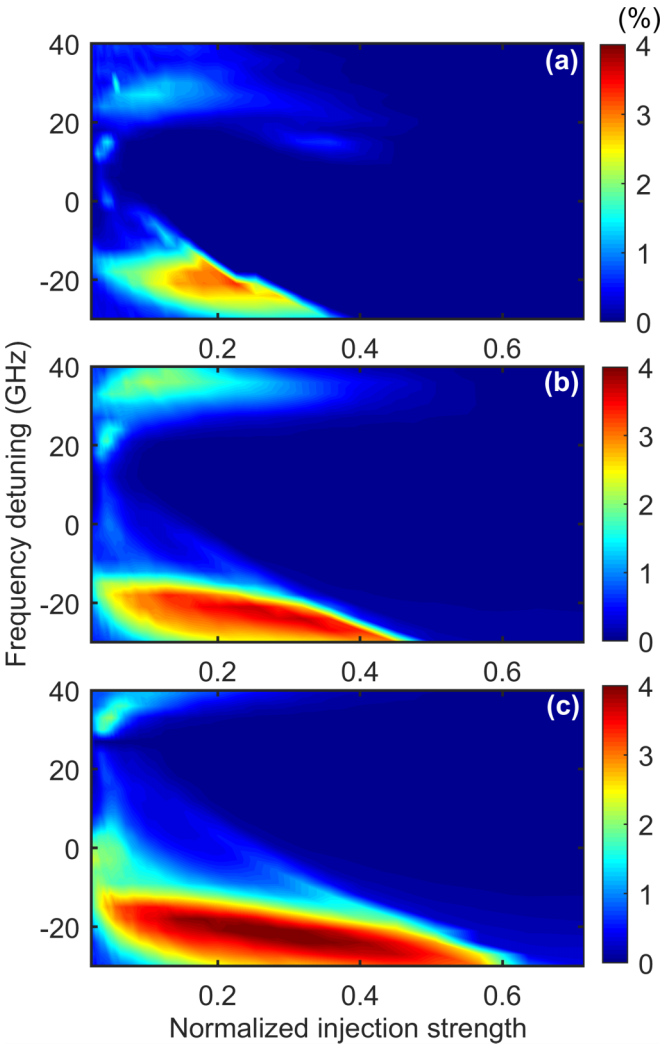

FIG. 6. Experimentally calculated color maps for the occurrence probability of EEs generated from the SL in the injection-parameter space. (a) $P_f = 0.12$ mW, (b) $P_f = 0.52$ mW, and (c) $P_f = 1$ mW. The right color bars represent the probability of EEs.

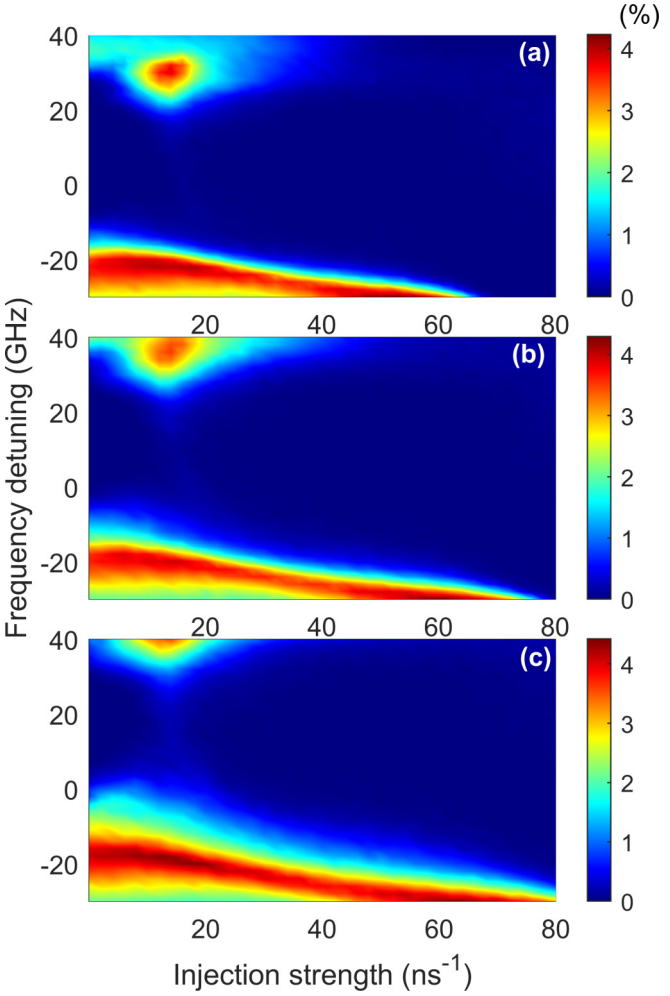

FIG. 7. Numerically calculated color maps for the occurrence probability of EEs generated from the SL in the injection-parameter space. (a) $k_f = 30$ ns^{-1}, (b) $k_f = 40$ ns^{-1}, and (c) $k_f = 50$ ns^{-1}. The right color bars represent the probability of EEs.

enhancement factor [36] is uncovered in Fig. 6(a). Compared with the case of positive detuning, a larger number of EEs can be easily achieved under the case of negative detuning. Moreover, we calculate the cross-correlation coefficient [15] between the ML and SL (not shown here). We discover that the regions for the enhanced EEs always appear in the areas without injection locking, where the SL dynamics can be tailored because of the interaction between the injection light from the ML and the field of the SL. Especially for certain negative detuning, the laser dynamics becomes more pulsing, showing a distinct departure from the ML output. That is, more fast oscillations close to the mean power can be found [e.g., see Fig. 4(a3)], which lowers the threshold of EEs, thus increasing the number of EEs detected. When the laser enters into the areas of injection locking, the occurrence probability of EEs trends to a stationary value. Again, the phenomena mentioned above are verified with the higher feedback power, as shown in Figs. 5(b) and 5(c). In the case with larger feedback powers, a blue region can be observed where the occurrence probability of EEs is lower than that generated from the ML, meaning that the generation probability of EEs decreased. Furthermore, with the increase of the feedback power, the region for the enhanced EEs located in the negative detuning is expanded in size; instead, the region for the enhanced EEs located in the positive detuning is transformed to a larger value of frequency detuning. This is attributed to the fact that the enhancement of the feedback power aggravates the asymmetry behavior in the master-slave configuration.

The experimental observations can also be understood in terms of the theoretical model given by Eqs. (1)–(6). To account for the limited bandwidth of the acquisition in the experiment setup, we perform a low-pass filter whose cutoff frequency is set at 15 GHz on the intensity time series of the laser output. Likewise, we focus on the effects of injection parameters on the generation of EEs, and the simulation results are shown in Fig. 7. From Fig. 7, two regions of the enhanced EEs can be found in the injection-parameter space. Moreover, we can also see that the appearance probability of EEs in the condition of negative detuning is much larger than that in the condition of positive detuning [see Fig. 7(b)].

This is mainly attributed to the enhancement of the interaction between the field of chaotic optical injection and the field of SL and the generation of new dynamic characteristics. These regions were also investigated for the improvement of chaotic complexity and bandwidth [37,38]. In addition, some dark-blue regions located in the range of injection parameters can be observed, in which the number of EEs is lower than that in the ML. This is mainly attributed to the fact the injection-locking mechanism is triggered with the increase of the injection strength. Our results show that experiments and simulations are almost perfectly consistent. Combining experiment and numerical results, we can conclude the following: (i) In the selected injection-parameter regions, where the injection-locking effect is not triggered, the occurrence probability of EEs can obviously be improved by adjusting the injection power and/or frequency detuning; on the contrary, triggering the injection-locking effect may maintain or even slightly reduce the appearance of EEs. (ii) In the regions of negative detuning, a larger number of EEs is gained compared with the case of positive detuning.

V. CONCLUSION

In conclusion, we have experimentally and numerically studied the evaluation of EEs in a semiconductor laser with chaotic optical injection, where a semiconductor laser with optical feedback in the long-cavity regime is deployed as a chaotic injection signal. Note that the deterministic optical RWs are observed in such a chaotic source operating in the long-cavity regime and such a chaotic source can easily be replaced by using another deterministic system. We carefully characterized the effects of injection parameters on the evolution of EEs. The results show that the appearance probability of EEs can be significantly enhanced in the regions of selected injection parameters. In contrast, we can expect that the EEs can be maintained or even slightly decreased when the injection-locking mechanism is triggered. Additionally, the occurrence probability of EEs in the negative detuning is much higher than that in the positive detuning. Our findings can be extended to other systems for researching RWs, in which a similar response to external forcing has been discovered.

ACKNOWLEDGMENTS

This work was supported by the National Natural Science Foundation of China (NSFC; Grants No. 62004135, No. 62001317, and No. 62171305), the Natural Science Research Project of Jiangsu Higher Education Institutions (Grants No. 20KJA416001 and No. 20KJB510011), and the Natural Science Foundation of Jiangsu Province (Grant No. BK20200855).

[1] C. Kharif and E. Pelinovsky, Eur. J. Mech. B **22**, 603 (2003).
[2] C. Kharif, E. Pelinovsky, and A. Slunyaev, *Rogue Waves in the Ocean* (Springer, Heidelberg, 2009).
[3] D. R. Solli, C. Ropers, P. Koonath, and B. Jalali, Nature (London) **450**, 1054 (2007).
[4] J. M. Dudley, F. Dias, M. Erkintalo, and G. Genty, Nat. Photonics **8**, 755 (2014).
[5] J. M. Dudley, G. Genty, A. Mussot, A. Chabchoub, and F. Dias, Nat. Rev. Phys. **1**, 675 (2019).
[6] J. Xu, J. Wu, J. Ye, J. Song, B. Yao, H. Zhang, J. Leng, W. Zhang, P. Zhou, and Y. Rao, Photonics Res. **8**, 1 (2020).
[7] M. Närhi, B. Wetzel, C. Billet, S. Toenger, T. Sylvestre, J.-M. Merolla, R. Morandotti, F. Dias, G. Genty, and J. M. Dudley, Nat. Commun. **7**, 13675 (2016).
[8] A. Klein, G. Masri, H. Duadi, K. Sulimany, O. Lib, H. Steinberg, S. A. Kolpakov, and M. Fridman, Optica **5**, 774 (2018).
[9] S. A. Kolpakov, H. Kbashi, and S. V. Sergeyev, Optica **3**, 870 (2016).
[10] O. Spitz, J. Wu, A. Herdt, G. Maisons, M. Carras, W. Elsäßer, C.-W. Wong, and F. Grillot, Adv. Photonics **2**, 066001 (2020).
[11] A. K. D. Bosco, D. Wolfersberger, and M. Sciamanna, Opt. Lett. **38**, 703 (2013).
[12] D. Choi, M. J. Wishon, J. Barnoud, C. Y. Chang, Y. Bouazizi, A. Locquet, and D. S. Citrin, Phys. Rev. E **93**, 042216 (2016).
[13] C.-H. Uy, D. Rontani, and M. Sciamanna, Opt. Lett. **42**, 2177 (2017).
[14] Y. Zeng, P. Zhou, Y. Huang, and N. Li, Opt. Lett. **47**, 142 (2022).
[15] J. Ahuja, D. B. Nalawade, J. Zamora-Munt, R. Vilaseca, and C. Masoller, Opt. Express **22**, 28377 (2014).
[16] P. Walczak, C. Rimoldi, F. Gustave, L. Columbo, M. Brambilla, F. Prati, G. Tissoni, and S. Barland, Opt. Lett. **42**, 3000 (2017).
[17] J. A. Reinoso, J. Zamora-Munt, and C. Masoller, Phys. Rev. E. **87**, 062913 (2013).
[18] M. W. Lee, F. Baladi, J.-R. Burie, M. A. Bettiati, A. Boudrioua, and A. P. A. Fischer, Opt. Lett. **41**, 4476 (2016).
[19] X. Li, X. Zhou, Y. Gu, and M. Zhao, IEEE J. Sel. Top. Quantum Electron. **28**, 0600108 (2022).
[20] S. Coulibaly, M. G. Clerc, F. Selmi, and S. Barbay, Phys. Rev. A **95**, 023816 (2017).
[21] C. Bonatto, M. Feyereisen, S. Barland, M. Giudici, C. Masoller, J. R. Rios Leite, and J. R. Tredicce, Phys. Rev. Lett. **107**, 053901 (2011).
[22] J. Zamora-Munt, B. Garbin, S. Barland, M. Giudici, J. R. Rios Leite, C. Masoller, and J. R. Tredicce, Phys. Rev. A **87**, 035802 (2013).
[23] S. Perrone, R. Vilaseca, J. Zamora-Munt, and C. Masoller, Phys. Rev. A **89**, 033804 (2014).
[24] T. Jin, C. Siyu, and C. Masoller, Opt. Express **25**, 31326 (2017).
[25] D. Choi, M. J. Wishon, C. Y. Chang, D. S. Citrin, and A. Locquet, Chaos **28**, 011102 (2018).
[26] Z. Zhong, D. Chang, W. Jin, M. W. Lee, A. Wang, S. Jiang, J. He, J. Tang, and Y. Hong, Photonics Res. **9**, 1336 (2021).
[27] J.-X. Dong, J.-P. Zhuang, and S.-C. Chan, Opt. Lett. **42**, 4291 (2017).
[28] R. Zhang, P. Zhou, Y. Yang, Q. Fang, P. H. Mu, and N. Q. Li, Opt. Express **28**, 7197 (2020).
[29] A. Uchida, *Optical Communication with Chaotic Lasers* (John Wiley & Sons, New York, 2012).
[30] M. Tlidi and K. Panajotov, Chaos **27**, 013119 (2017).

[31] C. Rimoldi, S. Barland, F. Prati, and G. Tissoni, Phys. Rev. A **95**, 023841(2017).
[32] M. Onorato, S. Residori, U. Bortolozzo, A. Montina, and F. T. Arecchi, Phys. Rep. **528**, 47 (2013).
[33] A. Wolf, J. B. Swift, H. L. Swinney, and J. A. Vastano, Phys. D (Amsterdam, Neth.) **16**, 285 (1985).
[34] É. Mercier, A. Even, E. Mirisola, D. Wolfersberger, and M. Sciamanna, Phys. Rev. E. **91**, 042914 (2015).
[35] N. Q. Li, H. Susanto, B. Cemlyn, I. D. Henning, and M. J. Adams, Opt. Lett **42**, 3494 (2017).
[36] Y. Huang, P. Zhou, and N. Li, Opt. Express **29**, 19675 (2021).
[37] P. H. Mu, W. Pan, and N. Li, Opt. Express **26**, 15642 (2018).
[38] S. Y. Xiang, W. Pan, B. Luo, L. S. Yan, X. H. Zou, N. Q. Li, and H. N. Zhu, IEEE J. Quantum Electron. **48**, 1069 (2012).